Is hydrogen gas in water present as bubbles or hydrated form?

メタデータ	言語: English
	出版者:
	公開日: 2016-03-24
	キーワード (Ja):
	キーワード (En):
	作成者: Aoki, K., Toda, H., Yamamoto, J., Chen, J., Nishiumi, T.
	メールアドレス:
	所属:
URL	http://hdl.handle.net/10098/9868

Is hydrogen gas in water present as bubbles or hydrated form?

Koichi Aoki*, Hirokazu Toda, Junpei Yamamoto, Jingyuan Chen, Toyohiko Nishiumi

Department of Applied Physics, University of Fukui,

3-9-1 Bunkyo, Fukui, 910-8507 Japan

Abstract

When hydrogen gas is bubbled into water, it may well be present as stabilized bubbles rather than hydrated hydrogen molecules, as in the spontaneous emulsification at oil|water interfaces without surfactant. On this prediction, we used dynamic light scattering (DLS) to find bubbles 0.4-0.5 μm in diameter, which were stable for more than 9 h. The intensity of the scattering light, which was proved to be proportional to concentrations of polystyrene latex suspensions, was also kept in solution in contact with hydrogen gas atmosphere. The bubbles were stable even at 50 g (gravity) by centrifugation. Voltammograms of the bubble-included solution had the oxidation peak, of which current was proportional to the intensity of DLS. Concentration of hydrogen in solution was evaluated accurately by comparing voltammetric currents at a regular electrode and a small electrode. The oxidation of hydrogen should be caused by the hydrated hydrogen which was supplied by dissolution of bubbles. Kinetic data of the dissolution were obtained at microelectrodes by using the advantage of extracting kinetics from diffusion currents. Voltammetric currents at microelectrodes were smaller by ten times than those predicted from diffusion of hydrated hydrogen. Therefore, the oxidation is controlled by the dissolution rate at the high current density. The rate was estimated to be 2×10^{-8} mol s^{-1} cm^{-2}, which was converted to the linear transfer rate, 0.4 mm s^{-1}, at gas|water interface.

key word: voltammetry of hydrogen; dissolution of gas; dynamic light scattering; centrifugation; microelectrode voltammetry;

---

* Corresponding author, e-mail kaoki@u-fukui.ac.jp (K. Aoki)

1. Introduction

Electrochemical oxidation of hydrogen gas dispersed in aqueous solution is a basic process of fuel cells of hydrogen [1,2]. The oxidation mechanism has been investigated mainly in acidic solutions [3-5]. It is composed of the two steps; the first including the formation of adsorbed hydrogen on a surface of metal M to yield MH [5-7]

$H_2 + 2M \leftrightarrow 2MH$ (Tafel reaction) or

$H_2 + M \leftrightarrow MH + H^+ + e^-$ (Heyrovsky reaction)
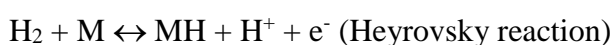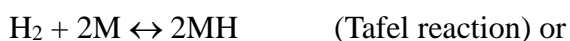
and the second including the electrochemical oxidation of MH

$MH \leftrightarrow M + H^+ + e^-$ (Volmer reaction)
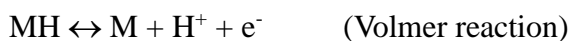
Which is favorable, the Tafel type or Heyrovsky one, depends on exposure of single crystal surface of platinum in solutions [8-10]. The latter seems to be favorable at multi-crystal surfaces [7]. Before the two-step reactions, there should be the dissolution process:

$$H_2(bubble) + nH_2O \rightarrow H_2(nH_2O) \tag{1}$$

through which a given concentration of hydrogen in water can be sustained. This process may also be one of rate-determining steps for real fuel cells. The oxidation has been challenged from a new concept in ionic liquids [11].

The dissolution equilibrium of gases is expressed by Henry's law [12]. Reported values of saturated hydrogen gas at 1 atm are 0.56 mM (M = mol dm^{-3}) and 0.63 mM, respectively, in 1.1 M aqueous NaCl solution and 0.2 M aqueous BaCl$_2$ solution [13-15]. Henry's law constants or Bunsen absorption coefficients, which determine solubility, have been evaluated from measurements of concentrations in solution and of partial pressures [16-18]. The accurate measurements have been performed by use of piezoelectric pressure sensors [19], pressure transducers [20] and differential pressure indicators [21], although they have disadvantage of a long lapse. Short time determination of solubility has been made by use of variations of volume or pressure reaching the saturated state [22-26]. Convenient and rapid measurements of solubility of hydrogen gas is potentiometry and amperometry of the electrochemical oxidation of

hydrogen [15,27,28]. The determination of the solubility always assumes equilibrium of reaction (1).

When water phase came in quiescent contact with oil phase, each phase near the boundary contained droplets of foreign phase [29,30]. Self-emulsification has been found even in bulk phase [31-34]. Droplet size was rather uniform. The uniform distribution has been demonstrated theoretically by statistical mechanics of various droplets whose oil|water surface tension was balanced with entropy of droplets [35]. This theory can be extended to gas|liquid surface without a loss of generality. Then it is predicted that hydrogen gas not only dissolves in water to hydrated molecules but also is dispersed in bubble form on a macroscopic scale. If the amount of hydrogen in the bubble form is higher than that in the hydrated form, the electrochemical oxidation of hydrogen may be controlled by the step of reaction (1) rather than the Heyrovsky reaction or the Volmer reaction. Furthermore, formation of stable bubbles may influence applications of hydrogen bubbles to some electrochemical techniques [36-38]. Under this question, we try to examine formation of hydrogen bubbles by combining dynamic light scattering, centrifugation and cyclic voltammetry.

2. Experimental

Aqueous solution saturated with hydrogen gas was prepared by bubbling hydrogen gas into 0.5 M KCl solution in a gas-sealed vessel from a hydrogen cylinder for 15 min at 20ºC at the atmospheric pressure. Hydrogen gas used was commercially available, with the purity of 99.99 %.

A potentiostat, HECS-1112 (Fuso, Kawasaki) was used for cyclic voltammetry. Platinum electrodes including microelectrodes were purchased (BAS, Tokyo). The reference and the counter electrodes were Ag/AgCl (3 M KCl) and platinum wire, respectively.

The size distribution was determined by a dynamic light scattering (DLS) instrument (Malvern Zetasizer Nano-ZS, UK). A centrifuge was SRX-201 (Tomy, Tokyo), which kept temperature of samples at 4 ºC.

Polystyrene latex particles were synthesized by the previous method by controlling compositions and mixing speeds [39].

3. Results and discussion

3.1. Detection of stable hydrogen bubbles

The hydrogen gas was bubbled into distilled water for 15 min, and the air-sealed cell was mounted on the DLS instrument. The size-distribution of the DLS signal had a peak, as shown in the inset of Fig. 1. The diameters were almost kept constant in 9 h when the solution was in contact with the hydrogen gas atmosphere (in Fig. 1 (circles)). The average diameter was 0.43 ± 0.04 μm, where the error means the standard deviation. The peak of the distribution demonstrates only the presence of any kind of micro-particles, but does not identify hydrogen bubbles. In fact, water into which oxygen, nitrogen, air or hydrogen gas was bubbled always showed a peak similar to in Fig. 1. The other possible source of the DLS signals is solid or liquid particles contained in the hydrogen gas, called aerosol. In order to remove possible contaminants, the gas was passed through a water bath before preparing hydrogen-included solutions. The DLS signal did not change with the insertion of the water bath. As a further confirmation, hydrogen gas was passed first through a methanol bath, then through the water bath. The DLS signal was also independent of this purification method.

An absolute value of the intensity of the scattering light is available as kcps (kilo-count per second) in the DLS instrument. It is expected to be proportional to the number of dispersed particles if the size is uniform. In order to find the relation, we used polystyrene latex particles with common size. Four kinds of polystyrene latex were synthesized in house [39], and the diameters of the dried latex and of wet latex were determined by SEM and DLS, respectively. Diameter values by the both methods were almost the same. Values of kcps were obtained for various number concentrations of latex suspensions, which were estimated by weight of dried latex, the volume of one latex particle, the density (1.04 g cm^{-3}) of polystyrene, and volume of the suspension. Figure 2 shows logarithmic plots of kcps values against the number concentrations, c_p,

of the latex. Values of kcps were proportional to the concentrations, exhibiting no significant intercept values (a few kcps). All the slopes of the lines were 1.00 ± 0.02. Therefore, we obtained the relation, kcps = (const) c_p. The value of (const), which was determined by the intercept in Fig. 2, had linear relations with logarithms of the diameters of the latex, as shown in Fig. 3. The slope was 3.77. The theoretical value by the Rayleigh scattering is six under the condition that particles are much smaller than the wavelength of light. Values of kcps and diameters of bubbles were independent of a type of nozzles (capillaries 0.5 - 2 mm in inner diameter and sintered glass with average pore size 0.3 mm) and gas flow rates. We use the following empirical expression from Fig. 3

$$[kcps] = 4.6 \times 10^{-5} \, c_p \, (2r)^{3.77} \tag{2}$$

where the unit of c_p is the number of particles per mm^3, and that of r is μm. The values of 4.6×10^{-5} and 3.77 may depend on physical properties of scattering particles through reflective coefficients. However it is helpful for order estimation of concentration of hydrogen bubbles from kcps and $2r$.

Values of kcps decreased with the time for 2 h, and then were kept constant (in Fig. 1 (triangles)). The decrease for the first 2h may be related with the slight decrease in $2r$, as can be realized through Eq. (2). When we insert the values of kcps and $2r$ of the bubbles into Eq. (2), neglecting the reflective coefficients in Eq. (2), we obtain 10^7 - 10^8 numbers of bubbles per mm^3. These values correspond to averaged molar concentration with the order of 0.1 mM of hydrogen molecule under 1 atm at 25°C. A bibliographic value of the saturated concentration of hydrogen is 0.56 mM [15].

Concentration of bubbles may be controlled by centrifugation, as has been conventionally used for control of concentrations of colloidal particles in suspensions. We centrifuged hydrogen-bubbled water at several accelerations for 10 min, and measured kcps. Figure 4 shows variations of kcps with the acceleration. The kcps values decreased with an increase in the acceleration to approach a given value rather than zero. This variation supports the stability of bubbles in water. It was difficult to remove bubbles completely by centrifugation. The difficulty may be ascribed to making the volume of bubbles small at high pressure or high acceleration to decrease the buoyancy. If aerosol were to be included in the gas, it should have settled out by the centrifugation

to decrease kcps values rapidly to zero. Diameters and kcps values were almost independent of concentration of KCl or HCl.

According to the quasi-equilibrium theory [35], the stability of bubbles is sustained by competition of a decrease in the surface tension of gas|water interface and thermal fluctuation. It can also be maintained by electric charge on bubbles [40]. The charging, however, does not conform to our system, because ions in the electrolyte (0.5 M KCl) neutralize the charge of bubbles.

3.2. Electrochemical Oxidation of hydrogen

Figure 5 shows the voltammogram of hydrogen-bubbled aqueous solution at the Pt electrode 1.6 mm in diameter, exhibiting a clear anodic peak. In contrast, the acid solution including hydrogen-bubbles showed a cathodic wave of hydrogen ion in addition to the anodic wave (not shown). The potentials of the both peaks varied, according to the Nernst equation. The reduction at a slow scan rate blocked the cathodic current, probably because the generated hydrogen is adsorbed on the electrode. Therefore we used 0.5 M KCl solutions in order to simplify the analysis of current-voltage curve of the oxidation current. The voltammograms at scan rates, v, less than 0.02 V s^{-1} had an anodic peak at -0.36 V vs. Ag|AgCl and a cathodic peak at -0.45 V. In contrast, a small anodic wave was superimposed on the anodic wave at -0.30 V for $v > 0.1$ V s^{-1}. Potentials of the main anodic and cathodic peaks were independent of scan rates for 0.01 $v < 1.0$ V s^{-1}. The anodic peak currents were approximately proportional to $v^{1/2}$ in this scan domain. The relation was empirically expressed by I_p /μA = 43.5(v / V s^{-1})$^{1/2}$ + 1.3. Figure 5 also shows the nearly steady-state voltammogram at the Pt electrode 0.1 mm in diameter, exhibiting the limiting current, I_L. A part of the current voltage curve, 0.1 < I /I_L < 0.9, was plotted in the form of log($I/(I_L - I)$) against the potential. The plot fell on a line, of which inverse slope was 40-45 mV. Since this value lay between 60 mV for a one-electron reaction and 30 mV for a two-electron reaction, the oxidation should not be of the combination of the Tafel reaction + the Volmer reaction, but must be close to the Heyrovsky type.

6

The oxidation of hydrogen proceeds as two-electron exchange reactions such as Heyrovsky reaction and the Volmer one, complicated by adsorption through the Tafel reaction. Diffusion-controlled currents at slow scan rates or steady-state voltammograms are generally proportional to v^q for $0.0 < q < 0.5$, whereas the adsorption currents are to v. Therefore, the peak current or the steady-state limiting current in the present experiments has less influence of adsorption steps. In order to analyze the slope of $\log(I/(I_L - I))$ against the potential, an expression for current-voltage curves with sequential two-electron transfer reactions is required. We derived the expression under the assumption of reversible two-electron reactions in the appendix. According to Eq. (AP4), the oxidation current, I, at the dimensionless potentials, $\zeta_1 = F(E - E_1^o)/RT$ and $\zeta_2 = F(E - E_2^o)/RT$ is given by

$$\ln \frac{I}{I_L - I} = \zeta_1 + \ln \frac{1 + 2e^{\zeta_2}}{2 + e^{\zeta_1}}$$

(3)

In the extreme case for $E_1^o \gg E_2^o$, this equation is approximated to $\ln[I/(I_L - I)] \approx 2F[E - (E_1^o + E_2^o)/2]/RT$, which suggests the concomitant two-electron reaction. Values of $\log(I/(I_L - I))$ were calculated from Eq.(3) for various values of E and $E_1^o - E_2^o$, and were plotted against E. The plots fell almost on a line for $0.1 < I/I_L < 10$ and $E_1^o - E_2^o < 0.07$ V. The values of the inverse slopes were plotted against $E_1^o - E_2^o$ in Figure 6. The plot was used as a working curve for evaluating $E_1^o - E_2^o$. By use of the experimental value of the slope, 0.043 V of the log plot, we determined $E_1^o - E_2^o = -0.013$ V.

Voltammetric peak current of a one-electron transfer reaction under the diffusion control is expressed by $0.446AFc^*(DvF/RT)^{1/2}$ [41], where A is the area of the electrode, and D is the diffusion coefficient. The peak current for a concomitant two-electron reaction for $E_1^o \gg E_2^o$ is $2^{3/2}(= 2.8)$ times larger than that for the one-electron, whereas that for a sequential two-electron reaction for $E_1^o \approx E_2^o$ is twice. The factor $2^{3/2}$ in the Randles-Sevcik equation can be attributed to varying the concentration ratio of the concomitant reaction at a double scan rate through the Nernst equation. The peak current ought to vary with values of $E_1^o - E_2^o$. The theoretical voltammograms for any value of $E_1^o - E_2^o$ can be given by replacing the current-voltage relationship for a one-electron transfer [42] by Eq. (AP4) to yield

$$j = c^*F\sqrt{\frac{DFv}{\pi RT}} \int_{-\infty}^{\zeta} \left(\frac{d}{d\zeta'} \frac{1}{1 + e^{\zeta_1'} + e^{\zeta_1' + \zeta_2'}} \right) \frac{d\zeta'}{\sqrt{\zeta - \zeta'}}$$

We carried out the numerical integration for several values of E_1^o - E_2^o, and plotted the peak current ratio, I_{p2}/I_{p1}, for the two-electron transfer, I_{p2}, to the one-electron transfer, I_{p1}, against E_1^o - E_2^o in Figure 6. The ratio tends to $2^{3/2}$ (= 2.8) for $E_1^o \gg E_2^o$, as predicted. The current ratio at the experimental value, E_1^o - E_2^o = -0.013 V, is 2.36. Then the peak current of the two-electron reaction for E_1^o - E_2^o = -0.013 V at the disk electrode in radius a_r (regular size) is expressed by

$$I_{p2} = 2.36 \times 0.446 \pi a_r^2 Fc* \sqrt{DvF/RT}$$

(5)

The steady-state limiting current of the two-electron reaction at a microelectrode in radius a_m is independent of values of E_1^o - E_2^o, and is given by

$$I_L = 8Fc*Da_m \tag{6}$$

When we take ratios of $I_{p2}v^{-1/2}$ to I_L and $(I_{p2}v^{-1/2})^2$ to I_L, we have, respectively

$$\frac{I_{p2}v^{-1/2}}{I_L} = \frac{0.413a_r^2}{a_m\sqrt{D}}\sqrt{\frac{F}{RT}}$$

(7)

(8)

$$\frac{\left(I_{p2}v^{-1/2}\right)^2}{I_L} = \frac{1.37a_r^4F^2c*}{a_mRT}$$

The value $I_{p2}v^{-1/2}$ was obtained from the slope of the plot of I_{p2} against $v^{1/2}$ for $2a_r = 1.6$ mm. In contrast, the value of I_L at $2a_m = 0.1$ mm was obtained from the intercept of the plot of the limiting currents against $v^{1/2}$ [43], because the limiting currents increased slightly with the scan rates. From known values on the left hand side in Eq. (7) and (8), we evaluated $c* = 0.50$ mM and $D = 4.6 \times 10^{-5}$ cm^2 s^{-1} independently. The value of $c*$ is close to the bibliographic value (0.56 mM [15]).

3.3. Dissolution of hydrogen gas from bubbles

When the cell was open to air, the anodic voltammogram of hydrogen gas was deformed slightly and the current decreased with the measurement time. This variation may be ascribed to replacement of hydrogen by oxygen in air and/or removal of hydrogen. When the cell was exposed to nitrogen atmosphere in a glove box, the

voltammogram was not deformed but the anodic peak current decreased with the time, as shown in Fig. 7. The half-life of the hydrogen gas was 1 h in the open cell 15 cm^3 in volume and 3 cm in depth. If hydrogen in water were to be in hydrated form, the replacement of hydrogen by nitrogen should be controlled by diffusion of hydrated hydrogen to or from the gas|water interface. The thickness of the diffusion layer in an hour might be 0.2 cm for the value of the diffusion coefficient 10^{-5} cm^2 s^{-1}. This value is much smaller than the depth of the cell (3 cm). Therefore, the replacement in the open cell should be caused by floating of bubbles rather than diffusion of hydrated hydrogen.

It is predicted that the anodic current has a close relationship with concentrations of bubbles. We decreased concentrations of bubbled solution by centrifugation at several accelerations (in Fig. 4), and soon carried out both voltammetry and DLS measurements. Figure 8 shows variations of the anodic peak currents with background-corrected values of kcps. The proportional relation indicates that the anodic current should be caused by transport of the hydrogen bubbles. If the transport were to be only diffusion of hydrogen bubbles, the current at a microelectrode would be expressed by

$$I_{\mathrm{L}} = 8enc_{\mathrm{p}}D_{\mathrm{b}}a_{\mathrm{m}}$$

(9)

where D_{b} is the diffusion coefficient of the bubble, and n is the number of hydrogen molecules per bubble. The value of n was obtained from the volume of a bubble and the equation of state of ideal gas. By use of the following numerical values $c_{\mathrm{p}} = 3\times10^{-7}$ mm^{-3}, $n = 1.1\times10^6$, $D_{\mathrm{b}} = 1.1\times10^{-8}$ cm^2 s^{-1} from the Stokes-Einstein's equation, we obtain $I_{\mathrm{L}} = 2$ pA at $2a_{\mathrm{m}} = 0.1$ mm. This is so small that diffusion of bubbles does not contribute to the current at all.

When hydrogen gas phase comes in contact with an electrode, the gas cannot be oxidized on the contacting part of the electrode, because no double layer is formed at the gas|electrode interface in the gas phase. It is the hydrated hydrogen molecule and/or hydrogen gas at the three-phase interface [44,45] that can be oxidized. Three-phase boundary reactions occur only when gas or oil including reactants is adsorbed on the electrode. We found that bubbles did not attach themselves on the electrode when the electrode was moved in the solution. Bubbles which were forced to be mounted on the

electrode were soon detached by weak mechanical vibration. Then the anodic current did not vary before and after the mount. Therefore no reaction at the three-phase boundary occurs. The anodic current should be primarily caused by dissolved hydrogen molecules.

If hydration reaction (1) is slower than the diffusion rate of hydrated hydrogen, it may be detected at high scan voltammetry as a decrease in the anodic current. This prediction can be supported by the positive intercept of the current in the plot, I_p /μA = 43.5$(v$ / V s$^{-1})^{1/2}$ + 1.3. Fast scan voltammograms higher than 1 V s^{-1} are too complicated for us to analyze quantitatively because of capacitive currents, uncompensated resistance and a delay of a potentiostat. The other technique of providing high current density is microelectrode voltammetry and hydrodynamic voltammetry under the steady state. We used here the former. Voltammograms of the oxidation of hydrogen at electrodes with diameter less than 0.1 mm were under the steady state at v < 20 mV s^{-1}. The limiting currents were compared with the theoretical diffusion-controlled current for the two-electron oxidation at radius a of the electrode [46]:

$$I_{th} = 8Fc*Da(0.34\mathrm{e}^{-0.66p} + 0.66 - 0.13\mathrm{e}^{-11/p} + 0.352p) \hspace{2cm} (10)$$

where $p = a$ $(vF/RTD)^{1/2}$. Figure 9 shows logarithmic plot of the experimental values of the limiting current, I_{exp}, against the theoretical ones, I_{th}. The experimental values for $2a$ ≥ 0.1 mm agreed with the theoretical ones, as shown on the dashed line with the slope 1. In contrast, those for $2a$ < 0.1 mm were smaller than I_{th}. The small deviation supports the rate-determining step of reaction (1). Especially, the ratio I_{exp}/I_{th} was 0.1 for $2a$ = 0.01 mm. This indicates [H$_2$(nH$_2$O)] < 10[H$_2$(bubble)]. Therefore most of hydrogen gas in water takes the dispersed bubble form rather than hydrated molecules.

This flux, $(8c*Da)/10(\pi a^2)$, should be controlled by the dissolution rate of hydrogen gas to water through the gas|water interface of bubbles. The dissolution rate considered here is the rate of mass per area of the gas|water interface of bubbles. We estimate the order of the dissolution rate constant in a hemisphere in radius a at a disk microelectrode. The hemisphere corresponds to the diffusion layer according to the conventional definition of the thickness, $Fc*D/j = (\pi/4)a \approx a$. Let the number of bubbles included in the hemisphere be m. Then moles of gas bubbles with radius r in the

hemisphere under the ideal gas state at the pressure P is given by $(P/RT)(4\pi/3)r^3m$. In contrast, moles of H_2 present in the hemispherical diffusion layer is expressed by $(2\pi/3)a^3c^*$. From the mass balance, both expressions should be equal. Then we have $m = (a/r)^3(RT/P)c^*/2$, from which the total surface area of bubbles is estimated to be $s = m(4\pi r^2) = 2\pi c^*(RT/P)a^3/r$. The numerical value of s is 43 μm^2 for $c^* = 0.5$ mM, $T = 298$ K, $P = 1$ atm, $2a = 0.01$ mm and $2r = 0.44$ μm. The bubbles are dissolved to water through this area to be oxidized electrochemically at the rate, $8c^*Da/10$. Letting the molar dissolution rate constant be k_d, we obtain the equality, $8c^*Da/10 = k_d s$, which yields $k_d = 2\times10^{-8}$ mol s^{-1} cm^{-2}. If this value is divided by c^*, we have the linear dissolution rate, 0.4 mm s^{-1} through gas|water interface. This rate is comparable to the flux of the voltammetric peak current at a large electrode ($I_p/Ac^*F = 1.05(DvF/RT)^{1/2}$) for $v = 0.8$ V s^{-1} and $2a_m = 5$ μm at a microelectrode ($I_L/Ac^*F = 8D/\pi a_m$). The dissolution rate is too fast to evaluate accurately the current by conventional voltammetry.

Conclusions

The answer of the title is that hydrogen in water is present favorably as gas bubbles rather than dissolved hydrogen. This result was obtained qualitatively from the distributions of macroscopic particles in gas-bubbled solution but also quantitatively from the kcps values which were proportional to the concentrations of macroscopic particles. The bubbles were stable for more than 9 h in the air-sealed vessel. They were sustained in a vessel against floatation even at the acceleration of 50 g.

The maximum concentration of hydrogen gas in water was determined voltammetrically by comparing the regular electrode and the electrode 0.1 mm in diameter. The determination required the derivation of the expression for the diffusion-controlled current of the partially concomitant two-electron reaction. The current was proportional to kcps values, implying the proportionality of concentrations of hydrated molecules to those of bubbles. Steady-state currents at microelectrode voltammetry were smaller than the theoretical values of the diffusion-controlled currents. The smaller values are ascribed to dissolution kinetics of gas to water (Eq. (1)). The dissolution rate constant is approximately 2×10^{-8} mol s^{-1} cm^{-2}.

Appendix

We derive here the expression for the steady-state current vs. voltage curve caused by a partially concomitant two-electron transfer reaction. When redox species, A_1, A_2 and A_3 are in electrochemical equilibrium with one electron transfer reactions:

$A_1 \leftrightarrow A_2 + e^-$ (standard potential: E_1°) (AP1)

$A_2 \leftrightarrow A_3 + e^-$ (standard potential: E_2°) (AP2)
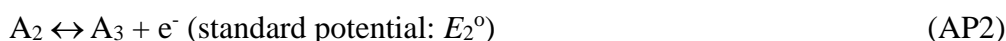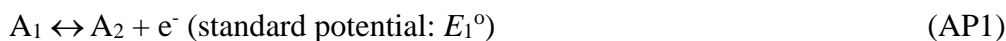
Nernst equations for the equilibrium reactions are

$$\zeta_1 \equiv (E - E_1^\circ)F / RT = \ln(c_2 / c_1)$$

$$\zeta_2 \equiv (E - E_2^\circ)F / RT = \ln(c_3 / c_2)$$

where c_i (i =1, 2, 3) are concentrations of A_i. Concentrations in consecutive reactions under the steady-state is satisfied by $c^* = c_1 + c_2 + c_3$, according to the mass balance [47,48]. Then each concentration is expressed by

$$c_1 = c^*/(1+e^{\zeta_1} + e^{\zeta_1+\zeta_2}),\ c_2 = c^* e^{\zeta_1} /\left(1+e^{\zeta_1} + e^{\zeta_1+\zeta_2}\right),\ c_3 = c^* e^{\zeta_1+\zeta_2} /\left(1+e^{\zeta_1} + e^{\zeta_1+\zeta_2}\right)$$

Since reactions $A_1 \rightarrow A_2$ and $A_1 \rightarrow A_3$ transfer one and two electrons, respectively, the charges that are required for formation of A_2 and A_3 should be proportional to c_2 and $2c_3$, respectively. The oxidation current is also proportional to $c_2 + 2c_3$. Replacing c_1, c_2 and c_3 by c^*, ζ_1 and ζ_2 yields

$$I = k(c_2 + 2c_3) = kc^* e^{\zeta_1}\left(1 + 2e^{\zeta_2}\right)/\left(1 + e^{\zeta_1} + e^{\zeta_1+\zeta_2}\right)$$ (AP3)

where k is the proportional constant. The limiting current of the oxidation, which occurs for $\zeta_1 \rightarrow \infty$ and $\zeta_2 \rightarrow \infty$, is given by $I_L = 2kc^*$. Then Eq. (AP3) is rewritten as

$$\frac{I}{I_L - I} = \frac{e^{\zeta_1}\left(1 + 2e^{\zeta_2}\right)}{2 + e^{\zeta_1}}$$ (AP4)

List of Symbols

A area of electrode

a radius of the electrode

a_m radius of disk microelectrode

a_r radius of the regular electrode (0.8 mm)

c^* bulk concentration of hydrogen gas

c_p concentration of particles or bubbles

D diffusion coefficient of hydrogen gas

D_b diffusion coefficient of bubbles

E electrode potential

E_1^o formal potential of the first step of the consecutive reaction

E_2^o formal potential of the second step of the consecutive reaction

F Faraday constant

g gravity

I anodic current at a potential E

I_L anodic limiting current of hydrogen under the steady state at microelectrodes

I_p peak current of anodic wave

I_{exp} voltammetric diffusion-controlled peak current by experiment

I_{th} voltammetric diffusion-controlled peak current by theory

j current density

kcps   kilo-count per second in the DLS instrument

k_d dissolution rate constant of hydrogen gas to the molecules

m number of bubbles included in the hemisphere

n number of hydrogen molecules included in a hydrogen bubble

P pressure of gas

p dimensional variable of the radius of the microelectrode

R gas constant

r radius of micro-particles

s total surface area of bubbles

T temperature

v potential scan rates

ζ_i dimensionless potential, $(E - E_i^o)/RT$, for the i step reaction

Acknowledgement

References

[1] R. O'Hayre, S.-W. Cha, W. Colella, F. B. Prinz, Fuel Cell Fundamentals, John Wiley and Sons, New York, 2006.

[2] H. Li, K. Lee, J. Zang, in PEM Fuel Cell Electrocatalysts and Catalyst Layers (ed. J. Zhang), Springer-Verlag, London, 2008, Chapter 3.

[3] M. W. Breiter. Electrochemical Processes in Fuel Cells, Springer, Berlin (1969).

[4] J. A. Harriso, Z. A. Khan, J. Electroanal. Chem. 30 (1971) 327.

[5] W. Vogel, I. Lundquist, P. Ross, P. Stonehart, Electrochim. Acta 20 (1975) 79.

[6] S. Shuldiner, J. Electrochem. Soc. 107 (1960) 452.

[7] R. M. Q. Mello, E. A. Ticianelli, Electrochim. Acta 42 (1997) 1031.

[8] E. Protopopoff, P. Marcus, J. Chim. Phys. 88 (1991) 1423.

[9] N. M. Markovic, P. Jr. Ross, Electrocatalysis at Well-defined Surfaces in Interfacial Electrochemistry, ed. A. Wieckowsky, Marcel Dekker, New York, 1991, pp. 821-842.

[10] N. M. Markovic, P. N. Ross, Surf. Sci. Rep. 45 (1002) 117.

[11] D.S. Silvester, L.Aldous, C. Hardacre, R.G. Compton, J. Phys. Chem. B 111 (2007) 5000.

[12] P.W. Atkins, Physical Chemistry, Sixth edition, Oxford University Press, Oxford, 1998, p. 173.

[13] J. Kumelan, A. P.-S. Kamps, D. Tuma, G. Maurer, Fluid Phase Equil. 260 (2007) 3.

[14] S. Horstmann, A. Grybat, R. Kato, J. Chem. Thermodyn. 36 (2004) 1015.

[15] R. R. Raposo, E.Calvino, M. A. Esteso, J. Electroanal. Chem. 617 (2008) 157.

[16] R. Battino, H.L. Clever, Chem. Rev. 66 (1966) 395.

[17] B.B. Benson, D. Krause, J. Chem. Phys. 64 (1976) 689.

[18] T. R. Rettich, Y. P. Handa, R. Battino, E. Wilhelm, J. Phys. Chem. 85 (1981) 3230.

[19] K. Fischer, M. Wilken, J. Chem. Thermodyn. 33 (2001) 1285.

[20] J. Kumelan, A. P.-S.o Kamps, I. Urukova, D. Tuma, G. Maurer, J. Chem. Thermodyn. 37 (2005) 595.

[21] T.R. Rettich, R. Brttino, E. Wilhelm, J. Chem. Thermodyn. 32 (2000) 1145.

[22] B.M. Moudgil, P. Somasundaran, I. Lin, J. Rev. Sci. Instrum. 45(1974) 406.

[23] T. Tominaga, R. Battino, H.K. Gorowara, R.D. Dixon, E. Wilhelm, J. Chem. Eng. Data 31 (1986) 175.

[24] M. Kato, K. Aizawa, T. Kanahira, T. Ozawa, J. Chem. Eng. Jpn. 24(1991) 767.

[25] M.C.C. Serra, A.M.F. Palavra, J. Solution Chem. 32 (2003) 527.

[26] A.M.A. Dias, R.P. Bonifacio, I.M. Marrucho, A.A.H. Padua, M.F.Costa-Gomes, Phys. Chem. Chem. Phys. 5 (2003) 543.

[27] J.J. Podesta, C.N. Estrella, M.A. Esteso, Sensor Actuator. B 32 (1996) 27.

[28] R. Bouchet, E. Siebert, G. Vitter, J. Electrochem. Soc. 147 (2000) 3125.

[29] K. Aoki, M. Li, J. Chen, T. Nishiumi, Electrochem. Commun. 11 (2009) 239.

[30] M.Li, K. Aoki, J. Chen, T. Nishiumi, J. Electroanal. Chem. 655 (2011) 159.

[31] Y. A. Shchipunov, O. Schmiedel, Langmuir 12 (1996) 6443.

[32] S. Pautot, B. J. Frisken, J.-X. Cheng, X. S. Xie, D. A. Weitz, Langmuir, 19 (2003) 10281.

[33] H. Gonza´lez-Ochoa, L. Ibarra-Bracamontes, J. L. Arauz-Lara, Langmuir 19 (2003) 7837.

[34] S. Sacanna, W. K. Kegel, A. P. Philipse, Langmuir 23 (2007) 10486.

[35] K. Aoki, J. Colloid Interface Sci. 360 (2011) 256.

[36] C.Huang, Yi-J. Li, C. Muangphat, Y. Hao, Electrochim. Acta 56 (2011) 8319.

[37] H. Van Parys, G. Telias, V. Nedashkivskyi, B. Mollay, I. Vandendael, S. Van Damme, J. Deconinck, A. Hubin, Electrochim. Acta 55 (2010) 5709.

[38] C. Brussieux, Ph. Viers, H. Roustan, M. Rakib, Electrochim. Acta 56 (2011) 7194.

[39] H. Chen, J. Chen, K. Aoki, T. Nishiumi, Electrochim. Acta 53 (2008) 7100.

[40] G. H. Kelsall, S. Y. Tang, A. L. Smith, S. Yurdakul, J. Chem. Soc. Faraday Trans. 92 (1996) 3879.

[41] R. S. Nicholson, I. Shain, Anal. Chem. 36 (1964) 706.

[42] K. Aoki, Electroanalysis, 17 (2005) 1379.

[43] H. Zhang, K. Aoki, J. Chen, T. Nishiumi, H. Toda, E. Torita, Electroanalysis, 23 (2011) 947.

[44] P. Tasakorn, J. Chen, K. Aoki, J. Electroanal. Chem. 533 (2002) 119.

[45] K. Aoki, P. Tasakorn, J. Chen, J. Electroanal. Chem. 542 (2003) 51.

[46] K. Aoki, K. Akimoto, K. Tokuda, H. Matsuda, J. Osteryoung, J. Electroanal. Chem. 171 (1984) 219.

[47] I. Ruzic, J. Electroanal. Chem. 52 (1974) 331.

[48] K. Aoki, J. Chen, J. Electroanal. Chem. 380 (1995) 35.